Origin of energy dispersion in $Al_xGa_{1-x}N/GaN$ nanowire quantum discs with low Al content

L. Rigutti,[1,*] J. Teubert,[2] G. Jacopin,[1] F. Fortuna,[3] M. Tchernycheva,[1] A. De Luna Bugallo,[1] F. H. Julien,[1] F. Furtmayr,[2,4] M. Stutzmann,[4] and M. Eickhoff[2]

[1]*Institut d'Electronique Fondamentale, University of Paris Sud XI, UMR 8622 CNRS, 91405 Orsay, France*

[2]*I. Physikalisches Institut, Justus-Liebig-Universität, Heinrich-Buff-Ring 16, 35392 Giessen, Germany*

[3]*Centre de Spectroscopie Nucléaire et Spectroscopie de Masse, University of Paris Sud XI, UMR 8609 CNRS, Bat. 108, 91405 Orsay, France*

[4]*Walter-Schottky-Institut, Technische Universität München, Am Coulombwall 3, 85748 Garching, Germany*

(Received 10 July 2010; revised manuscript received 6 October 2010; published 6 December 2010)

Individual GaN nanowires containing $Al_xGa_{1-x}N/GaN$ quantum discs (QDiscs) with Al content $x \leq 16\%$ have been investigated by microphotoluminescence, transmission electron microscopy, and theoretical modeling. Single quantum discs show narrow emission lines with a linewidth as low as 3 meV at energies above the GaN band gap while the emission of nanowires containing multiple quantum discs shows multiple peaks with total spectral broadening that depends on the Al content in the barrier. As assessed by simulations of the quantum confinement based on a three-dimensional effective-mass model, the main factors influencing the spectral dispersion are: (i) strain relaxation in the QDiscs, strongly affected by the presence of a lateral AlGaN shell with a progressively changing thickness formed during the barrier growth; (ii) monolayer fluctuations in the QDisc thickness.

DOI: 10.1103/PhysRevB.82.235308 PACS number(s): 78.40.Fy, 78.55.Cr

I. INTRODUCTION

Quantum discs (QDiscs) embedded in nanowires (NWs) have recently gathered considerable attention due to the properties distinguishing them from two-dimensional quantum well layers and Stranski-Krastanov quantum dots. These structures can be grown without dislocations and offer a more efficient strain management for the development of light emitters and single photon sources.[1,2]

The growth of GaN nanowires containing Al(Ga)N/GaN QDiscs has been successfully demonstrated using catalyst-free molecular-beam epitaxy (MBE).[3,4] The ensembles of Al(Ga)N/GaN QDiscs have been shown to produce broad photoluminescence at energies higher than the GaN band gap. The important broadening of their emission was theoretically explained by the size dispersion from wire to wire and also by the strain relaxation along the nanowire axis, the internal field in the QDiscs and the band bending at the nanowire surfaces.[3,5,6] Theoretical analyses predict a variation in the band gap and a reduction in the internal piezoelectric field due to the relaxation of strain at the lateral surface.[7] Narrow photoluminescence lines originating from AlN/GaN single-QDisc structures have been demonstrated by microphotoluminescence (μ-PL).[1] However, no such analysis has been performed for low Al content AlGaN/GaN QDiscs. The latter system exhibits a much lower internal electric field than pure AlN/GaN heterostructures resulting in better luminescence efficiency. Moreover, a QDisc system with low Al content is better suited for luminescence devices under electrical injection. Therefore it is of particular interest for optoelectronic applications such as nanoscale light emitters. Single nanowire emission in AlGaN/GaN systems has only been probed by microcathodoluminescence.[6] However, narrow emission related to single QDisc could not be observed due to peak broadening produced by strong electron-beam excitation.

In the present work we have investigated the relation between structural and optical properties of $Al_xGa_{1-x}N/GaN$ single or multiple QDiscs (MQDiscs) with low Al content ($x \leq 0.16$) embedded in single GaN nanowires. μ-PL experiments reveal several narrow emission lines (with linewidth as low as 3 meV) above the GaN band-gap energy for MQDisc samples with $x=0.16$ while a large emission peak is found for the sample with $x=0.05$. The analysis shows that the QDisc emission lines are spread over an energy interval which increases with the Al content in the barriers. Transmission electron microscopy (TEM) was performed on all samples and in selected cases directly correlated with μ-PL measurements on the same nanowire. The results of the structural TEM analysis were used as input parameters for the simulation of the confined electronic states in the framework of a three-dimensional (3D) effective-mass model. The calculations take into account the QDisc thickness fluctuation, the variation in the strain state along the nanowire axis, the presence of an external AlGaN shell with progressively changing thickness and the effect of band bending induced by the pinning of the Fermi level on the nanowire top and lateral surfaces. The combination of these effects, as well as the consideration of excitonic effects, well accounts for the observed emission energy and spectral dispersion of the narrow emission lines.

II. EXPERIMENTAL DETAILS

We analyzed two nanowire samples containing nine $Al_xGa_{1-x}N/GaN$ MQDiscs and a reference sample containing a single quantum disc. All samples were grown by catalyst-free plasma-assisted MBE on Si(111) substrates at a substrate temperature of 780 °C. Nitrogen-rich conditions were employed in order to achieve self-assembled nanowire growth. The nanowire axis corresponds to the *c*-polar axis of

the GaN lattice. Details on the growth technique can be found in Ref. 8.

The nominally undoped nanowires consist of a GaN base part, approximately 350–400 nm long, followed by an $Al_xGa_{1-x}N/GaN$ heterostructure and overgrown with a 20-nm-thick $Al_xGa_{1-x}N$ cap. The shape of the nanowire, as deduced from scanning electron microscopy, is that of a hexagonal prism. TEM analysis reveals a disc and barrier thickness in the MQDisc heterostructures of $t_{QD}=1.5-1.75$ nm ($t_{QD}=1-1.25$ nm) and $t_b=5.5$ nm ($t_b=6$ nm) in sample 1 (sample 2). The Al fraction in the barriers is $x=5\%$ ($x=16\%$) for sample 1 (sample 2). The Al fraction was determined by comparing the PL emission energy of a reference nanowire single heterostructures with thick AlGaN cap to values reported for AlGaN layers with known Al content.[9] The single QDisc reference sample has the same parameters as sample 2 except for the number of QDiscs. For all samples the nanowire height and diameter fluctuate from wire to wire between 400–450 nm and 25–60 nm, respectively.

After macro-PL characterization of the ensembles, nanowires were detached from the substrate by ultrasound bath in ethanol and dispersed on a Formvar-on-Carbon TEM membrane. The density of the nanowires was controlled by dispersion in the range of $1\times10^6-5\times10^6$ cm^{-2}, a suitable value for both μ-PL and transmission electron microscopy characterization.

Macro-PL and μ-PL characterization was carried out at $T=4.2$ K by exciting the sample with cw 244 nm light from a frequency-doubled Ar^{++} ion laser. The laser radiation was focused onto the substrate surface with a spot of diameter ~3 μm by means of a 20× UV microscope objective with 0.4 numerical aperture. The excitation power was kept in the range 50 μW–10 mW. The luminescence was collected with the same objective, dispersed with a 460 mm focal length spectrometer and detected with a charge coupled device. The spectral resolution of the system for a 600 grooves/mm grating is 500 μeV.

For the correlation of the TEM image and of the μ-PL spectrum from the same nanowire, nanowires were first analyzed by μ-PL. The position of isolated nanowire-related emissions, evidenced by a luminescence spot, was recorded by means of a visualization system. Then the MQDisc structures have been analyzed in high-resolution TEM (HR-TEM) in order to extract the structural parameters with an accuracy down to the atomic monolayer (ML). The uniformity of Al content in the barriers was verified by energy-dispersive x-ray analysis (EDX) throughout the whole quantum structure.

III. OPTICAL AND STRUCTURAL ANALYSIS

Figures 1(a) and 1(b) present the macro-PL spectra of nanowire ensembles of both MQDisc samples compared to selected μ-PL spectra of single wires. The samples show two main luminescence features: the one at 3.4–3.47 eV is the near-band edge (NBE) emission of the GaN base of the nanowires, the one at higher energy is attributed to the AlGaN/GaN MQDisc emission. For most nanowires the intensity of the GaN NBE features is lower than the intensity

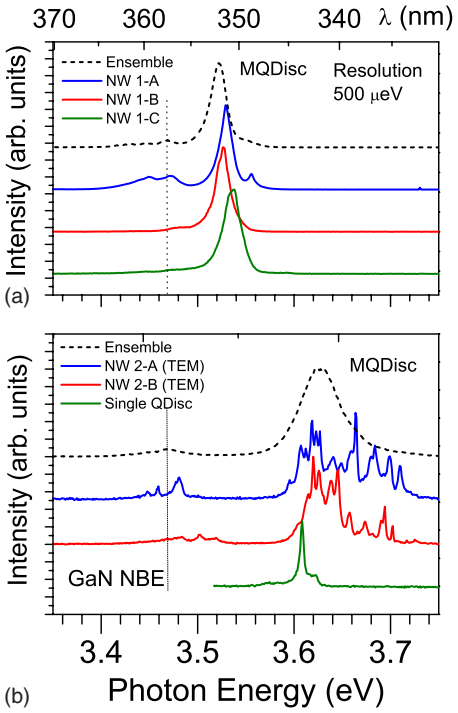

FIG. 1. (Color online) (a) The PL spectrum of the ensemble of the nanowires (dashed black line) and of isolated nanowire emissions (solid lines in color) from sample 1. (b) The PL spectrum of the ensemble of the nanowires (dashed black line) and of a set of single nanowires or nanowire bundles (continuous lines, in color) from sample 2. The green line (first from the bottom) corresponds to the spectrum of a nanowire with the same heterostructure parameters of sample 2 but containing a single QDisc. All spectra are normalized to the MQDisc maxima and vertically shifted for clarity.

of the signal from the MQDisc system. The MQDisc emission of the nanowire ensemble is peaked at $E_{MQD}=3.52$ eV with a full width at half maximum (FWHM) of 20 meV for sample 1. For sample 2, it is shifted to higher energy ($E_{MQD}=3.63$ eV) with an increased broadening of 45 meV.

For sample 1, the μ-PL spectra of single wires do not differ significantly from the spectrum of the ensemble. The MQDisc emission from single wires has a peak energy in the range $E_{MQD}=3.518-3.534$ eV with a FWHM of 12–16 meV. The linewidth is only slightly lower than the inhomogeneous broadening recorded for the ensemble showing that the spectral dispersion of the MQDisc emission from wire to wire is quite low. The MQDisc emission from a single nanowire is a superposition of the emission peaks of the nine individual QDiscs, which cannot be separately resolved. However, in some cases (for example, the spectrum of sample 1-A depicted in Fig. 1(a), narrow separate lines can be observed on the high-energy part of the spectrum.

In contrast to sample 1, the μ-PL spectra of single nanowires from sample 2 strongly differ from the ensemble emission. While the MQDisc PL of the ensemble exhibits a broad single peak at $E_{pk}=3.62-3.63$ eV with a FWHM of 45 meV, single nanowires show multiple narrow peaks with energies varying in the interval $E_{MQD}=3.59-3.73$ eV and a small spectral width of FWHM=3 meV. The narrow peaks in the spectra of sample 2 are attributed to the emission of indi-

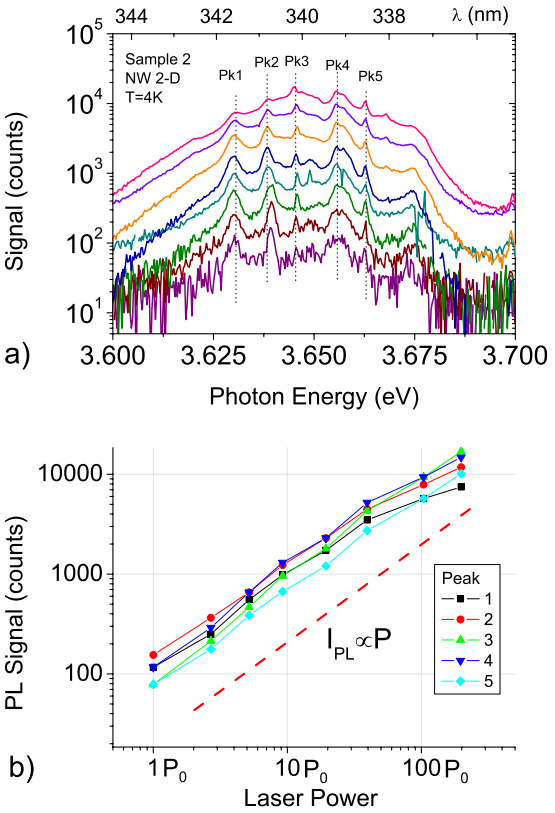

FIG. 2. (Color online) (a) μPL spectra taken at increasing power level from a single nanowire from sample 2 (NW 2-D) at $T=4$ K. (b) Dependence of the intensity of selected peaks on the power level. The quantity $P_0=50$ μW is the laser power transmitted by the microscope objective.

vidual QDiscs. This interpretation is confirmed by the μ-PL analysis of the reference sample containing a single QDisc (SQDisc), shown in Fig. 1(b). The high-energy emission consists of a single narrow peak in the same energy range as the peaks in sample 2. It should be noted that the linewidth of the SQDisc emission (FWHM=7 meV) is comparable to that of the individual peaks in the nanowires from sample 2. As deduced from polarization-resolved measurements performed on both samples, the symmetry of the MQDisc emission follows the polarization selection rules of the X_A exciton.[10]

Interestingly, for many single wires the number of PL peaks exceeds the number of QDiscs. For example, the spectrum of the nanowire 2-B containing nine QDiscs (Fig. 1) exhibits 12 narrow lines. Similarly, the spectrum of the single QDisc nanowire exhibits one main peak at $E=3.609$ eV and a second peak at $E=3.622$ eV.

Figure 2(a) reports power-dependent photoluminescence measurements in the spectral interval corresponding to QDisc emission for one single nanowire from sample 2. They reveal that the PL peak energy does not change and the peak intensity grows linearly when the excitation power is increased over two decades [Fig. 2(b)]. This linear dependence is a strong indication of the excitonic nature of the radiative transition.[11] No saturation is found within the investigated power interval.

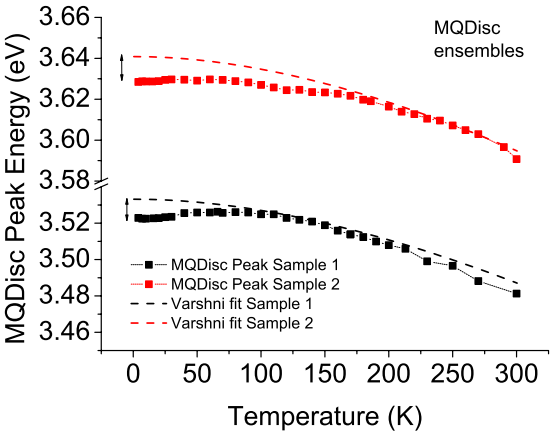

FIG. 3. (Color online) Temperature dependence of the PL energy of the ensembles of samples 1 (black squares) and 2 (red circles). The dotted lines correspond to the fit with the empirical Varshni model with parameters $E_{PL}(T)=E_{PL}(0)-6.7\times10^{-4}T^2/(T+874)$.

Figure 3 reports the temperature dependence of the PL peaks of the MQDisc emission of the ensembles of samples 1 and 2. For temperatures well above 150 K the blueshift of the PL energy with decreasing temperature can be well fitted by the semiempirical Varshni model $E_{PL}(T)=E_{PL}(0)-6.7\times10^{-4}T^2/(T+874)$. The fitting parameters used are the same reported in previous studies on $Al_xGa_{1-x}N/GaN$ quantum well structures with structural parameters very close to those of the QDiscs of this study.[12] For further temperature decrease a redshift of the PL emission is observed for both samples. This redshift has also been observed in AlGaN/GaN quantum well systems and can be assigned to exciton localization at local potential minima induced by alloy disorder at the well/barrier interface.[12]

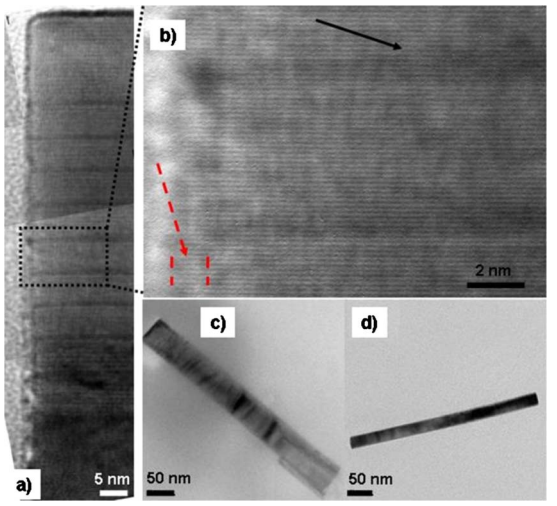

FIG. 4. (Color online) (a) HR-TEM image of the multi-QDisc region of one nanowire from sample 2. (b) Zoom of the region evidenced by the dashed rectangle in part (a); the black arrow shows the single monolayer fluctuation at one of the QDisc interfaces while the red dashed arrow evidences the AlGaN shell. TEM images of the nanowires correlated with the reported PL spectra from sample 2: (c) nanowire 2-A; (d) nanowire 2-B.

Figures 4(a) and 4(b) show high magnification TEM images of the MQDisc region in nanowire 2-A. The interfaces of the QDiscs are generally atomically flat. Isolated single monolayer steps are visible at the interfaces, as indicated by the arrow in Fig. 4(b). These steps are due to the incomplete formation of atomic monolayers during the growth of QDiscs and barriers. The extracted QDisc thickness is typically 6 or 7 ML for sample 1, 4, or 5 ML for sample 2, and 5 ML for the reference sample. QDiscs with local thickness of 5 ML (6 ML) have also been found in sample 1 (sample 2). Previous works performed on AlGaN/GaN nanowire heterostructures point out that lateral growth can lead to the formation of an AlGaN shell surrounding the MQDisc system.[4] The presence of such a shell is indicated both by HR-TEM [as visible in Fig. 4(b)] and EDX analyses which showed the presence of Al in the GaN base part of the nanowire. According to the HR-TEM images, the thickness of the shell increases in the nanowire 2-A from 0.3–0.5 nm in correspondence of the topmost QDisc to about 2 nm at the interface between the AlGaN barrier and the GaN base. The TEM images of nanowires labeled 2-A and 2-B are reported in Figs. 4(c) and 4(d), respectively. They show that nanowire 2-A (2-B) has a diameter (i.e., the diameter of the cylinder circumscribing the nanowire) d_w=51 nm (d_w=30 nm). Despite this difference the MQDisc emissions in wires 2-A and 2-B are distributed on similar energy intervals [Fig. 1(b)], which may indicate a weak influence of the nanowire diameter on the emission properties. The structural parameters measured by TEM have been used for the subsequent simulation of the electronic properties of these structures.[13]

IV. MODELING AND DISCUSSION

In order to elucidate the effect of quantum confinement and strain distribution on the variation in the MQDisc emission energies in samples 1 and 2, we have carried out numerical simulations based on a three-dimensional effective-mass model for self-consistent solution of the Schrödinger-Poisson equation in the QDiscs implemented in the software NEXTNANO^3.[14] The results are summarized in Fig. 5. The structural input parameters were extracted from TEM analysis[13] and a rectangular numerical mesh with a density of two mesh points per nanometer in each direction was used. A detailed list of the material parameters used in the simulation is reported in Table I.

For calculation of the strain distribution the integral elastic energy was minimized applying zero-stress boundary conditions at the NW surface[15] (achieved by defining a surrounding air cluster within NEXTNANO^3) and assuming fully coherent interfaces in accordance with theoretical considerations.[16]

As a main difference to previous reports[5,7] the strain is calculated throughout the whole MQDisc system and the presence of an AlGaN shell with identical composition as the barrier material and gradually decreasing lateral thickness from 1.0 nm for QDisc #1 (bottom) to 0.3 nm for QDisc #9 (top) is taken into account.

Figure 5(a) shows the calculated distribution of the ε_{zz} component of the strain tensor inside the QDiscs along the

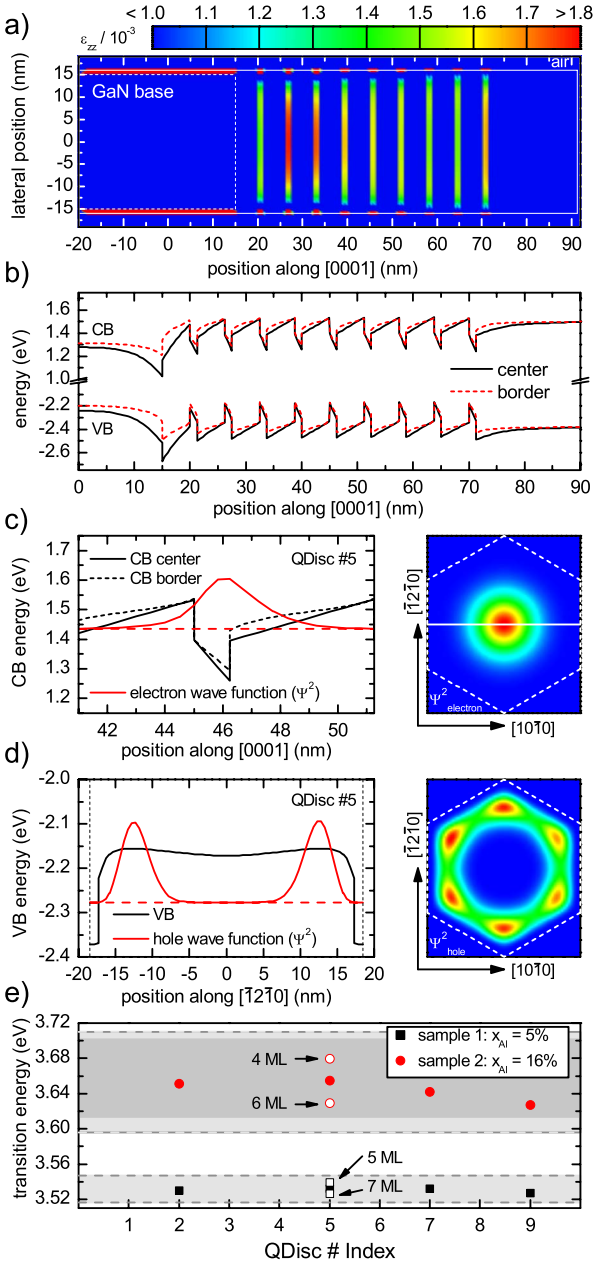

FIG. 5. (Color online) Simulation results for the structure of nanowire 2-B. (a) Distribution of the ε_{zz} strain tensor component in the QDiscs for the plane indicated by the solid white line in part (c) along the nanowire axis; (b) profile of CB and VB in the QDisc structure calculated along the nanowire axis and close to the boundary to the lateral AlGaN shell; (c) and (d) ground-state wavefunction profiles in QDisc #5. (c) Left: electron along the [0001] direction on the nanowire axis, right: contour plot of $|\Psi|^2$ in the (0001) plane; (d) left: hole along the $[\bar{1}2\bar{1}0]$ axis in the plane of the QDisc, right: contour plot of $|\Psi|^2$ in the (0001) plane; and (e) transition energy between ground states vs QDisc index calculated for sample 1, t_{QD}=1.5 nm (black squares) and for sample 2, t_{QD} =1.25 nm (red circles). Open symbols represent calculations performed for single monolayer fluctuations in QDisc #5. The gray region in the lower energy part of the plot corresponds to the dispersion of the main PL peak in sample 1 nanowires while the light (dark) gray region in the higher energy part of the plot corresponds to the dispersion of the PL peaks from nanowire 2-A (2-B).

TABLE I. Numerical parameters used in the simulation.

Parameter	Value as a function of x_{Al}
a (nm)	$0.3112x+(1-x)0.3189$
c (nm)	$0.4982x+(1-x)0.5185$
m^* perpendicular	$0.32x+(1-x)0.206$
m^* parallel	$0.30x+(1-x)0.202$
C_{11}	$396x+(1-x)390$
C_{12}	$137x+(1-x)145$
C_{13}	$108x+(1-x)106$
C_{33}	$373x+(1-x)398$
C_{44}	$116x+(1-x)105$
e_{33} (C/m^2)	$1.79x+(1-x)1.27$
e_{31} (C/m^2)	$-0.50x-(1-x)0.35$
e_{15} (C/m^2)	$-0.48x-(1-x)0.30$
Spontaneous polarization (C/m^2)	$-0.0340x-(1-x)0.0900-0.021x(1-x)$
a_1 (eV)	$-3.4-(1-x)4.9$
a_2 (eV)	$-11.8-(1-x)11.3$
D_1 (eV)	$-17.1-(1-x)3.7$
D_2 (eV)	$7.9+(1-x)4.5$
D_3 (eV)	$8.8+(1-x)8.2$
D_4 (eV)	$-3.9-(1-x)4.1$
D_5 (eV)	$-3.4-(1-x)4.0$
D_6 (eV)	$-3.4-(1-x)5.1$
ΔE_{CB} $GaN/Al_{0.05}Ga_{0.95}N$	130 meV
ΔE_{CB} $GaN/Al_{0.16}Ga_{0.84}N$	402 meV
ΔE_{CB} GaN/AlN	1.9248 eV
Doping	$E_D=20$ meV, $n=10^{17}$ cm^{-3}

axis of nanowire 2-B [in the plane indicated by the solid white line in Fig. 5(c), rhs]. The presence of the lateral shell reduces the radial strain variation inside each QDisc. However, the variation in the shell thickness along the wire enhances the strain gradient in the axial direction related to the elastic strain relaxation inside the QDiscs with increasing distance from the GaN base. This effect can be verified by performing the same calculation assuming a shell of constant thickness: in this case the strain state is almost homogeneous in the axial direction and hardly changes with QDisc index (not shown).[17]

For calculation of the resulting valence-band (VB) and conduction-band (CB) profiles, displayed for the QDisc region in Fig. 5(b), spontaneous polarization, strain-induced piezoelectric polarization, and the effect of deformation potentials have been taken into account.[18] The position of the Fermi level defines the "zero" potential. A homogeneous residual doping concentration of $N_d=10^{17}$ cm^{-3} is assumed. The Fermi-level pinning on the top and lateral surfaces was assumed to give rise to a surface band bending of 1.5 eV.[3,5,19,20] The consequences of this boundary condition and of the radial strain relaxation are visible in the plot of Fig. 5(b). The upward lateral surface band bending of both bands is most pronounced in QDisc #1 and decreases along the wire. Moreover, the resulting geometrical extension of the space-charge region prevents carriers from accumulating in the QDiscs and at the lower GaN/AlGaN heterointerface. This is in agreement with the results presented in Ref. 19, stating that nominally undoped GaN nanowires with a diameter below 80 nm can be considered as fully depleted due to the lateral extension of the space-charge region.

The polarization-induced internal electric field in the QDiscs is on the order of ~1000 kV/cm in the center and ~800 kV/cm at the edges of QDiscs in sample 2. In Ref. 21 internal electric fields of 710 kV/cm have been extracted indirectly for GaN quantum wells with an Al concentration of 17% in the barriers by modeling the evolution of the transition energy with quantum well thickness. The deviation from the present results can be due to the assumption of a perfect pseudomorphic growth in the simulation which neglects possible relaxation mechanisms, such as the formation of interfacial defects. In addition it should be noted that a direct comparison between the numerically obtained electric field strength in QDiscs and those obtained experimentally via comparison of PL transition energies in 2D quantum well structures with different height might be not justified due to the laterally inhomogeneous band profile in the QDiscs which might affect the geometry of the excitonic wave function.

In order to obtain an estimate for the PL transition energies, and in particular for their variation along the wire axis, the confined one-particle electron and hole states were calculated for QDisc numbers 2, 5, 7, and 9. Applying Dirichlet boundary conditions the Schrödinger equation was solved numerically for a "quantum region" (defined within NEXTNANO[3]) ranging from 4 nm below to 5 nm above the respective QDisc. The resulting lateral band profile induces a spatial separation of confined one-particle electron and hole states, preferentially localized in the center and at the border of the QDisc, respectively [shown for QDisc #5 in Figs. 5(c) and 5(d)]. However, the resulting in-plane electric field inside the QDiscs was found to be smaller than 30 kV/cm, i.e., it is not sufficient to overcome the electron-hole Coulomb interaction that is responsible for exciton formation.[22] This result suggests that for a QDisc height smaller than the exciton Bohr radius [3–3.4 nm for GaN (Refs. 23 and 24)], the QDisc luminescence should be described in terms of recombination of excitons rather than separated electron-hole pairs. This is in agreement with the observation that the emission energy does not vary with increasing excitation-power density while the PL intensity increases linearly. Therefore, the transition energies calculated using the one-particle wave functions provide an upper estimate and should be corrected to account for the exciton binding energy.[25] The exciton binding energy in the present MQDisc system can be approximated by a value of 50 meV according to reports on AlGaN/GaN quantum well systems.[12,21,25–27] An additional correction arises from the exciton localization at potential fluctuations caused, e.g., by alloy disorder at the QDisc interfaces or by point defects. An estimate for this correction can be extracted from the deviation of the low-temperature PL emission energies with respect to the empirical Varshni model (Fig. 3), which reveals a localization energy of 10–12 meV for both samples, similar to respective values reported for AlGaN/GaN quantum well systems.[12,27]

It is worth to notice that the one-particle states are well localized in the QDiscs in the case of sample 2 while in sample 1 there is a non-negligible leakage of the electron states into the $Al_{0.05}Ga_{0.95}N$ barrier, possibly giving rise to the formation of diagonal excitonic transitions[28] involving two neighboring QDiscs and yielding an additional broadening of the PL peak which can be estimated as ~5 meV.

Figure 5(e) reports the calculated transition energies between the ground state of electron and hole in selected QDiscs of sample 1 ($x_{Al}=5\%$, $t_{QD}=1.5$ nm) and sample 2 ($x_{Al}=16\%$, $t_{QD}=1.25$ nm) corrected by an exciton binding energy of 50 meV (Ref. 21) and a localization energy of 10 meV. The obtained variation along the wire axis is smaller for sample 1 ($\Delta E^{str}_{5\%}=5$ meV) than for sample 2 ($\Delta E^{str}_{16\%}=30$ meV) in agreement with experiment. If a homogeneous shell thickness of 0.3 nm is assumed for the latter case $\Delta E^{str}_{16\%}$ is reduced to 10 meV, emphasizing the importance of the inhomogeneous thickness of the surrounding shell as a main dispersion mechanism. It should be noted that the impact of the AlGaN shell on the energy dispersion is probably even underestimated in the present model. In fact, due to the different kinetics of Ga and Al atoms on the nonpolar sidewalls during growth,[4,29] the Al concentration in the shell might be higher than in the barrier material, resulting in a higher dispersion of the emission energies.

The second main dispersion mechanism is given by monolayer fluctuations of the QDisc height. The open symbols in Fig. 5(e) visualize variations in the respective transition energies due to monolayer fluctuations in the QDisc height for QDisc #5. For small Al concentrations (sample 1) these fluctuations induce a variation in transition energy of $\Delta E^{ML}_{5\%}=\pm 6$ meV, which significantly increases to $\Delta E^{ML}_{16\%}=\pm 28$ meV for an Al concentration of 16% (sample 2).

The dotted lines in Fig. 5(e) represent the width of the experimentally determined energetic distribution of the luminescence indicating reasonable agreement between the measured and calculated luminescence energies when considering shell effects and ML fluctuations. Further phenomena could play a role in the dispersion of the PL energies. Among those are variations in the exciton binding and localization energies, as well as the possibility for the exciton to bind at charged point defects. Nevertheless, these effects are not expected to be strongly dependent on the Al content in the barriers and their contribution should not be higher than the average value of the localization energy. A further minor dispersion factor could be related to the NW diameter, as NWs with larger diameter have a higher difference in the respective strain states on the axis and at the lateral edge, possibly enhancing the difference of the related transition energies. However, the comparison of the PL energy dispersion and the NW diameter measured on a larger number of NWs (~20) by scanning electron microscopy did not show a direct correlation of these two quantities.

The results strongly suggest that both the axial gradient of the shell thickness and the presence of monolayer fluctuations in the QDisc height are the main contributions to the variation in transition energies between different QDiscs within one nanowire and also result in the broadening of the ensemble luminescence. It is important that both contributions are enhanced when the Al concentration in the barriers is increased. This is directly evidenced by the comparison of sample 1 and sample 2 in this work. For sample 1 with an Al concentration of 5% in the barriers, the variation in the transition energies in different QDiscs is comparable to the linewidth of individual QDisc emissions leading to an overlap of emission lines. Therefore, only one luminescence peak due to superposition of the contribution of different QDiscs is obtained in single wire PL measurements. Increasing the Al content in the barriers to 16% results in a stronger confinement making energy levels much more sensitive to geometrical stress, electric field, and any other variable changes. This translates into a larger difference of transition energies, so the emission of single QDiscs within one wire can be resolved.

Finally, it should also be noted that the number of QDiscs in the NW and the number of experimentally observed emission peaks do not necessarily have to coincide as localization of excitons at local potential minima can occur at different in-plane positions with different monolayer thickness, strain state, or localization energy. This also accounts for occurrence of more than one emission line in the case of SQDisc-NWs.

V. CONCLUSIONS

In conclusion, we performed a systematic combined characterization of the optical and structural properties of AlGaN/GaN QDiscs in GaN nanowires. Emission lines with FWHM as low as 3 meV corresponding to individual QDiscs were observed for moderate Al contents ($x=16\%$) in the heterostructure barriers. The transition energies of the individual QDiscs incorporated within the same nanowire present a significant variation along the wire. By comparison to numerical simulations we have identified monolayer fluctuations and an axial gradient of the lateral shell thickness as dominating mechanisms for the observed dispersion of the PL energy of the MQDiscs. For both mechanism, the resulting variation in transmission energies along the wire increases with increasing Al concentration in the barriers.

ACKNOWLEDGMENTS

This work was supported in part by the French ANR agency under Programs No. ANR-08-NANO-031 BoNaFo and No. ANR-08-BLAN-0179 NanoPhotoNit. The authors from JLU and WSI acknowledge financial support form the European Commission with the project DOTSENSE (Grant No. STREP 224212).

*Corresponding author; lorenzo.rigutti@ief.u-psud.fr

[1] J. Renard, R. Songmuang, C. Bougerol, B. Daudin, and B. Gayral, Nano Lett. **8**, 2092 (2008).
[2] A. Tribu, G. Sallen, T. Aichele, R. André, J.-P. Poizat, C. Bougerol, S. Tatarenko, and K. Kheng, Nano Lett. **8**, 4326 (2008).
[3] J. Ristić, E. Calleja, M. A. Sánchez-García, J. M. Ulloa, J. Sánchez-Páramo, J. M. Calleja, U. Jahn, A. Trampert, and K. H. Ploog, Phys. Rev. B **68**, 125305 (2003).
[4] M. Tchernycheva, C. Sartel, G. Cirlin, L. Travers, G. Patriarche, J. C. Harmand, L. S. Dang, J. Renard, B. Gayral, L. Nevou, and F. H. Julien, Nanotechnology **18**, 385306 (2007).
[5] J. Ristić, C. Rivera, E. Calleja, S. Fernández-Garrido, M. Povoloskyi, and A. Di Carlo, Phys. Rev. B **72**, 085330 (2005).
[6] U. Jahn, J. Ristić, and E. Calleja, Appl. Phys. Lett. **90**, 161117 (2007).
[7] C. Rivera, U. Jahn, T. Flissikowski, J. L. Pau, E. Munoz, and H. T. Grahn, Phys. Rev. B **75**, 045316 (2007).
[8] F. Furtmayr, M. Vielemeyer, M. Stutzmann, J. Arbiol, S. Estradé, F. Peirò, J. R. Morante, and M. Eickhoff, J. Appl. Phys. **104**, 034309 (2008).
[9] H. Angerer, D. Brunner, F. Freudenberg, O. Ambacher, M. Stutzmann, R. Höpler, T. Metzger, E. Born, G. Dollinger, A. Bergmaier, S. Karsch, and H.-J. Körner, Appl. Phys. Lett. **71**, 1504 (1997).
[10] L. Rigutti, M. Tchernycheva, A. De Luna Bugallo, G. Jacopin, F. H. Julien, F. Furtmayr, M. Stutzmann, M. Eickhoff, R. Songmuang, and F. Fortuna, Phys. Rev. B **81**, 045411 (2010).
[11] T. Schmidt, K. Lischka, and W. Zulehner, Phys. Rev. B **45**, 8989 (1992).
[12] M. Leroux, N. Grandjean, M. Läugt, J. Massies, B. Gil, P. Lefebvre, and P. Bigenwald, Phys. Rev. B **58**, R13371 (1998).
[13] See supplementary material at http://link.aps.org/supplemental/10.1103/PhysRevB.82.235308 for the Table I reporting the structural parameters measured by TEM and used for defining the structure in the numerical simulation can be found in Table A.
[14] See NEXTNANO website http://www.wsi.tum.de/nextnano3 for tutorial input files and detailed documentation.
[15] M. Povolotskyi and A. Di Carlo, J. Appl. Phys. **100**, 063514 (2006).
[16] F. Glas, Phys. Rev. B **74**, 121302 (2006).
[17] The calculations of the strain state were performed assuming $T=4$ K. According to [S. Figge, H. Kröncke, D. Hommel, and B. M. Epelbaum, Appl. Phys. Lett. **94**, 101915 (2009)], the estimated change in strain state between 4 K and RT due to the different thermal expansion of the AlGaN and GaN alloys is in the range of 5×10^{-5} for sample 2 and 2×10^{-5} for sample 1, which is negligible compared to the strain state inside the QDiscs (on the order of 10^{-3}).
[18] I. Vurgaftman and J. R. Meyer, J. Appl. Phys. **94**, 3675 (2003).
[19] R. Calarco, M. Marso, T. Richter, A. I. Aykanat, R. Meijers, A. d. Hart, T. Stoica, and H. Lüth, Nano Lett. **5**, 981 (2005).
[20] L. Ivanova, S. Borisova, H. Eisele, M. Dähne, A. Laubsch, and Ph. Ebert, Appl. Phys. Lett. **93**, 192110 (2008).
[21] N. Grandjean, B. Damilano, S. Dalmasso, M. Leroux, M. Läugt, and J. Massies, J. Appl. Phys. **86**, 3714 (1999).
[22] A. Shikanai, T. Deguchi, T. Sota, T. Kuroda, A. Tackeuchi, S. Chichibu, and S. Nakamura, Appl. Phys. Lett. **76**, 454 (2000).
[23] B. Gil and O. Briot, Phys. Rev. B **55**, 2530 (1997).
[24] M. Gallart, A. Morel, T. Taliercio, P. Lefebvre, B. Gil, J. Allègre, H. Mathieu, N. Grandjean, M. Leroux, and J. Massies, Phys. Status Solidi A **180**, 127 (2000).
[25] Excitonic effects cannot be included within the present version of NEXTNANO^3 for the special case of free-standing wurtzite NWs in a 3D calculation.
[26] M. Leroux, N. Grandjean, J. Massies, B. Gil, P. Lefebvre, and P. Bigenwald, Phys. Rev. B **60**, 1496 (1999).
[27] N. Grandjean, B. Damilano, J. Massies, G. Neu, M. Teissere, I. Grzegory, S. Porowski, M. Gallart, P. Lefebvre, B. Gil, and M. Albrecht, J. Appl. Phys. **88**, 183 (2000).
[28] B. Gil, P. Lefebvre, J. Allègre, H. Mathieu, N. Grandjean, M. Leroux, J. Massies, P. Bigenwald, and P. Christol, Phys. Rev. B **59**, 10246 (1999).
[29] J. Ristić, E. Calleja, A. Trampert, S. Fernández-Garrido, C. Rivera, U. Jahn, and K. H. Ploog, Phys. Rev. Lett. **94**, 146102 (2005).